Inorganic Chemistry

Article

Cite This: Inorg. Chem. 2019, 58, 9358−9367

pubs.acs.org/IC

From Ylides to Doubly Yldiide-Bridged Iron(II) High Spin Dimers via Self-Protolysis

Sivathmeehan Yogendra,* Thomas Weyhermüller, Anselm W. Hahn, and Serena DeBeer*

Max Planck Institute for Chemical Energy Conversion, Stiftstrasse 34-36, 45470 Mülheim an der Ruhr, Germany

Supporting Information

ABSTRACT: A synthetic strategy for the preparation of novel doubly yldiide bridged iron(II) high spin dimers ($[(\mu_2\text{-}C)FeL]_2$, L = $N(SiMe_3)_2$, Mesityl) has been developed. This includes the synthesis of ylide-iron(II) monomers [(Ylide)-FeL_2] via adduct formation. Subsequent self-protolysis at elevated temperatures by *in situ* deprotonation of the ylide ligands results in a dimerization reaction forming the desired bridging μ_2-C yldiide ligands in $[(\mu_2\text{-}C)FeL]_2$. The comprehensive structural and electronic analysis of dimers $[(\mu_2\text{-}C)FeL]_2$, including NMR, Mössbauer, and X-ray spectroscopy, as well as X-ray crystallography, SQUID, and DFT calculations, confirm their high-spin Fe^{II} configurations. Interestingly, the Fe_2C_2 cores display very acute Fe−C−Fe angles (averaged: 78.6(2)°) resulting in short Fe···Fe distances (averaged: 2.588(2) Å). A remarkably strong antiferromagnetic coupling between the Fe centers has been identified. Strongly polarized Fe−C bonds are observed where the negative charge is mostly centered at the μ_2-C yldiide ligands.

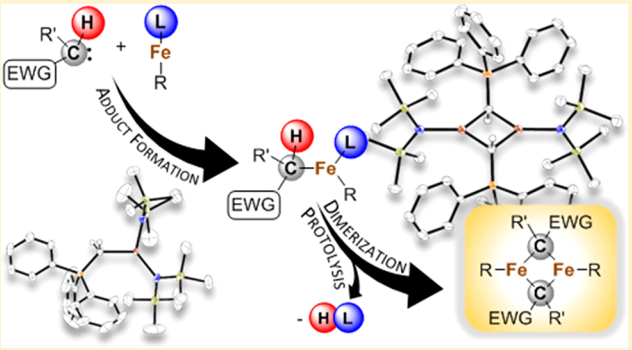

INTRODUCTION

Nitrogenases are the only enzymes that are capable of reducing atmospheric N_2 to NH_3.[1] This conversion occurs at a heterometallic Fe_7MoS_9C cluster, known as FeMoco, which contains a very unique interstitial μ_6-carbide ligand (Chart 1A).[2] Biosynthetically, the carbide ligand originates from the methyl group of S-adenosylmethionine and is transferred to the iron sulfur cluster via a radical mechanism.[3] While the role of the carbide ligand for the catalytic activity of the FeMoco is unknown, it has been postulated to function as a stabilizing anchor for the cluster,[4] to allow for facile modulation of the belt iron interactions during substrate binding,[5] and even to form transient C−H bonds during catalysis.[6] However, a detailed understanding of the exact role of the carbide is in part limited by the absence of any synthetic models which support both a μ_6-carbide ligand and locally high-spin ferrous (and ferric) iron atoms.[7] In fact, synthetic strategies that allow the introduction of C-based ligands bonded to more than one Fe atom (μ_{2-6}-C-based ligands) are very rare, explaining the lack of suitable model systems. Known strategies are, for example, the conversion or substitution of CO ligands in polyironcarbonyl clusters into μ_3-, μ_5-, or μ_6-C-ligands to yield, e.g., clusters of type B (Chart 1).[8] Unfortunately, these clusters contain strong-field CO ligands and are low-spin complexes, in contrast to the sulfide ligated high spin iron sites in FeMoco.

Carbido bridged, diamagnetic porphyrinato (C) and phthalocyanato Fe dimers have been synthesized using CI_4 as a μ_2-C^{4-} ligand source, yielding high-valent Fe^{IV} sites.[9] In addition, a dimeric but low spin $[1,2,4\text{-}^tBu(C_5H_2)Fe^{II}(\mu_2\text{-}CPh)]_2$ complex containing μ_2-C ligands was synthesized by alkyne insertion into an Fe═Fe double bond.[10] In addition, a small number of low coordinated, high spin Fe dimers bridged by singly charged μ_2-C^- ligands were prepared by using $(H_3C)Li$ or ArylLi as $[H_3C]^-$ and $[Aryl]^-$ sources functioning as two electron donor ligands.[11−13] Recently, Holland and co-workers have reported on the synthesis of the singly alkylidene bridged high-spin Fe^{II} dimer of type D by using diazoalkanes as a μ_2-C^{2-} ligand source, formally having been a four electron donor ligand.[14]

In this contribution, we report on the development of a new synthetic strategy for generating μ_2-C^{2-} yldiide ligands that support the coordination of high-spin iron, which enabled the preparation of novel doubly yldiide-bridged iron(II) high spin complexes. This has been accomplished by starting from novel low-coordinated Fe^{II}−ylide complexes of type E containing both a strongly basic ligand (L) and a H-acidic ylide ligand facilitating self-protolysis and subsequent dimerization yielding dinuclear complexes of type F. The well-established chemistry of isolable ylides containing, e.g., phosphonio or imidazoliumyl substituents as electron withdrawing groups (EWG) allows precise substituent adjustment,[15] rendering these as potential precursors for μ_2-C^{2-} ligands.

Received: April 14, 2019
Published: July 1, 2019

DOI: 10.1021/acs.inorgchem.9b01086
Inorg. Chem. 2019, 58, 9358−9367

Chart 1. Top: FeMo-Cofactor (A) and Other Nitrogenase Relevant Iron Clusters (B–D) Containing C-Based Ligands; Bottom: Synthetic Strategy to Form Doubly Yldiide Bridged Iron(II) High Spin Dimers

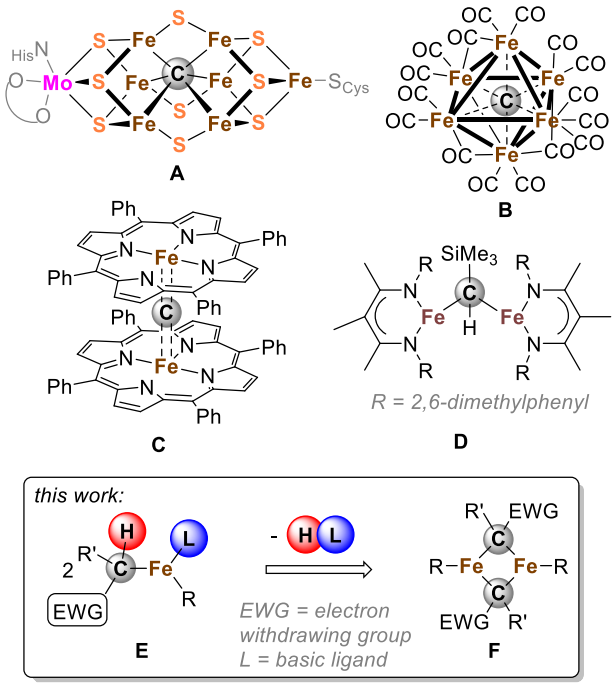

RESULTS AND DISCUSSION

The reaction of the phosphorus ylides **1a** and **1b** or the related N-heterocyclic olefin (NHO) **1c** with $[Fe(N(SiMe_3)_2)_2]$ results in the quantitative formation of the Fe^{II}–ylide adducts **2a–2c**, which are isolated in good yields (Scheme 1). The molecular structures for all three congeners were determined by X-ray crystallography and show a distorted trigonal planar coordination environment around the Fe atom (Figure 1). The N–Fe–N angles decrease with higher steric demand of the ylide (**1b** > **1a** > **1c**, see Table 1).[16]

Scheme 1. Preparation of Low Coordinated Fe^{II}–Ylide Complexes Containing Amide Substituents

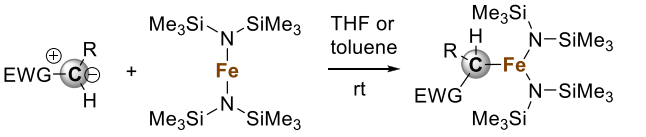

1a: EWG = Ph_3P, R = H
1b: EWG = Ph_3P, R = $SiMe_3$
1c: EWG = Im, R = H

2a: EWG = Ph_3P, R = H: 85%
2b: EWG = Ph_3P, R = $SiMe_3$: 81%
2c: EWG = Im, R = H, 52 %

Interestingly, the Fe–C bonds in all three Fe^{II}–ylide complexes which are at 2.158(6) Å (**2a**), 2.176(2) Å (**2b**), and 2.159(3) Å (**2c**), respectively, are longer than the Fe–C bond distances in the related tricoordinated alkyl substituted [LFeR] complexes reported by the groups of Hessen and Holland (L = bulky β-diketiminate ligand, R = Me, ^{i}Pr, $CH_2{}^t$Bu, benzyl; Fe–C: 2.009(3)–2.048(3) Å)[17] or in the anionic congener $[((Me_3Si)CH_2)Fe(N(SiMe_3)_2)_2]$-$[(THF)_3Na(NHC^{Dipp})]$, which is at 2.065 Å.[18] This observation points to a weaker donor strength of the ylide ligands. In the case of the Ph_3P substituted complexes **2a** and **2b**, this can be explained by the strong negative hyperconjugation of the lone pair of the ylidic C atoms into the σ^*–P–C^{Ph} bonds, as indicated by the shortened C–P bonds ($\sum_{covalent\_radii}$(C,P): 1.83 Å) of 1.751(6) Å and 1.736(1) Å in **2a** and **2b**, respectively.[19] In the NHO substituted complex **2c**, the ylidic lone pair is strongly involved in forming the π–C–C2 bond at 1.417(5) Å, which is in between the expected values for a C–C single bond (1.54 Å) and a double (1.34 Å) bond.[20] This delocalization decreases the overall ylide donor strength in **2c**.[15c] The widened Fe–C–P angles of 133.4(5)° and 120.35(7)° in **2a** and **2b**, respectively, can be explained by the steric repulsion of the Ph_3P and the $N(SiMe_3)_2$ groups. The paramagnetic character of complexes **2a–2c** is manifested in the broad and paramagnetically shifted resonances observed in their ^{1}H NMR spectra. No resonances could be found in the ^{31}P and ^{29}Si NMR spectra of **2a** and **2b** due to paramagnetism. The solution magnetic susceptibilities determined at room temperature by Evan's method[21] are calculated to be 4.9 μ_B, 5.2 μ_B, and 5.5 μ_B for **2a–2c**, respectively. These values are all close to the expected value of 4.9 μ_B for high-spin Fe^{II} complexes (S = 2). The ^{57}Fe Mössbauer spectra of **2a–2c** recorded at 80 K display isomer shifts ranging from δ = 0.51 to 0.55 mm/s (see Supporting Information (SI), Figures S9–S11), which are typical values for tricoordinated Fe^{II} centers in high-spin configurations and are comparable to the shift observed in [LFeMe] (L = bulky β-diketiminate ligand, δ = 0.48 mm/s).[17c] In contrast, the quadrupolar splittings of ΔE_Q = 0.92, 0.73, and 1.14 mm/s for **2a–2c**, respectively, deviate significantly from the quadrupole splitting of ΔE_Q = 1.74 mm/s determined for [LFeMe]. We note that no Mössbauer has

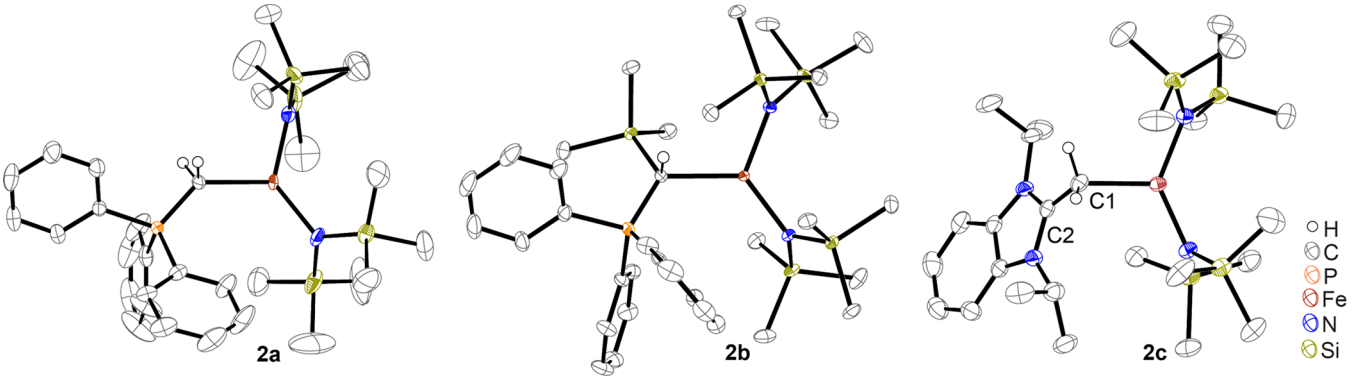

Figure 1. Molecular structures of **2a–2c**. Selected hydrogen atoms are omitted for clarity; thermal ellipsoids are displayed at 50% probability.

DOI: 10.1021/acs.inorgchem.9b01086
Inorg. Chem. 2019, 58, 9358–9367

Table 1. Selected Geometrical Parameters for the Crystallographically Characterized Iron Complexes 2a–2c (Bond Lengths in Å and Angles in Degrees)

	Fe–C	Fe–N		C–P/C2[b]	N–Fe–N	Fe–C–P/C2[b]	angle sum Fe
2a	2.158(6)	1.963(5)	1.962(5)	1.751(6)	127.8(4)	133.4(5)	359.8(11)
2b	2.176(1)	1.954(1)	1.970(1)	1.736(1)	122.63(5)	120.35(7)	359.7(2)
2c[a]	2.159(3)	1.939(3)	1.950(3)	1.417(5)	133.6(1)	115.2(2)	359.5(4)

[a]Two independent molecules in unit cell; only one molecule is considered due to nonsignificant differences in structural parameters. [b]C2 atom in complex **2c**.

been reported for the other known dialkyl- or diaryl-bridged diiron compounds.[11−13]

Complexes **2a–2c** are extremely air and moisture sensitive and readily decompose in solvents such as CH_2Cl_2, $CHCl_3$, and CH_3CN, which is probably due to the high reactivity of the weak Fe–C bond in **2a–2c**. This hypothesis is nicely corroborated by the formal insertion of benzonitrile into the Fe–C bond of **2a**. Subsequent proton migration from the ylidic C atom to the nitrile N atom yields complex **3** (Scheme 2). Due to its high reactivity and thermal instability

Scheme 2. Reaction of 2a with Benzonitrile

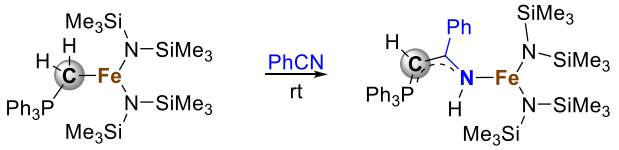

(decomposes at ambient temperature), **3** was not isolated in larger amounts. However, suitable single crystals for X-ray crystallography of **3** were obtained from a PhCN/*n*-pentane mixture at −35 °C showing the *E* isomer with a distorted trigonal planar coordination environment around the Fe atom (angle sum around Fe: 359.8(2)°; Figure 2). Both, the

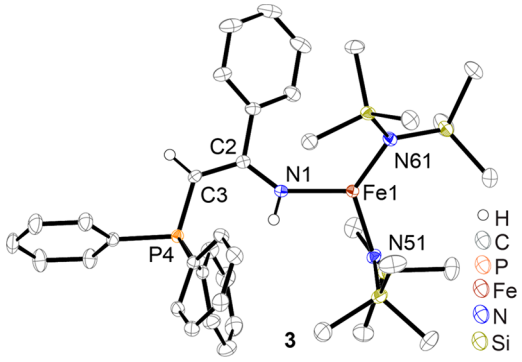

Figure 2. Molecular structure of **3** (selected hydrogen atoms omitted for clarity, thermal ellipsoids displayed at 50% probability). Selected bond lengths in Å and angles in degrees: Fe1–N1 2.018(1), Fe1–N51 1.949(1), Fe1–N61 1.945(1), N1–C2 1.328(2), C2–C3 1.398(2), C3–P4 1.723(1).

shortened N1–C2 (1.328(2) Å), C2–C3 (1.398(2) Å), and C3–P4 (1.723(1) Å) bond lengths in **3** as well as the planarity of the N1–C2–C3–P4 unit (torsion angle 0.1(3)°) indicate a significant π-delocalization over this fragment. The presence of basic amido- and a H-acidic ylide ligands in **2a–2c** should allow for an intramolecular deprotonation reaction generating an additional donor site at the ylide–C atom. Attempts to induce such a self-protolysis reaction by refluxing solutions of **2a–2c** in toluene, THF, or C_6H_5F were unsuccessful and yielded deep brown reaction mixtures of unidentified products. However, melting solid **2a** at 135 °C results in condensation of a colorless liquid at the glass wall and the formation of a brown sticky residue. The colorless product is identified as $HN(SiMe_3)_2$ (Scheme 3, I), while recrystallization of the brown

Scheme 3. Formation of Doubly Yldiide Bridged Fe^{II} Complexes via Self-Protolysis Reaction

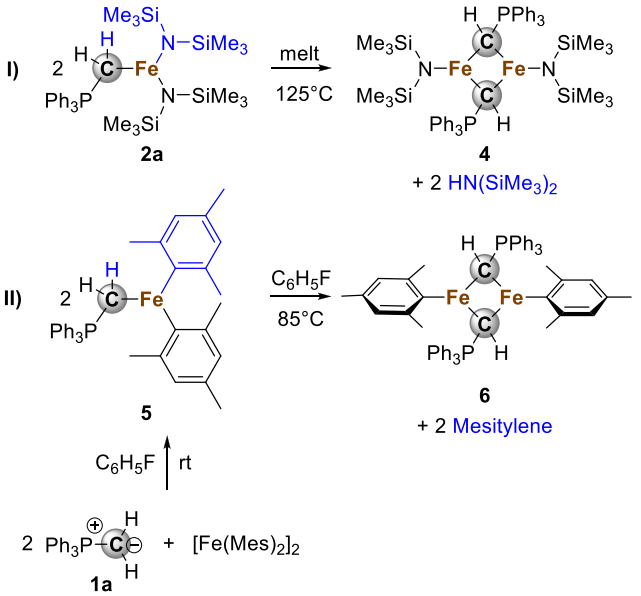

residue from CH_2Cl_2 results in the formation of analytically pure, orange-brown block-like crystals which are composed of the desired doubly yldiide-bridged Fe^{II} dimer **4** (isolated yield: 27%). Following the same synthetic approach for **2b** and **2c** resulted in the formation of an unidentifiable reaction mixture.

However, a second yldiide-bridged iron dimer can be prepared by reacting a fluorobenzene solution of **1a** with $[Fe(Mes)_2]_2$[13] (Mes = 2,4,6-trimethylphenyl) instead of $[Fe(N(SiMe_3)_2)_2]$ as an iron precursor. In analogy to the basic $N(SiMe_3)_2$ ligands, the mesityl ligands in $[Fe(Mes)_2]_2$ act as proton acceptors inducing the self-protolysis reaction (Scheme 3, II). Upon the addition of two equivalents of **1a** to a red solution of $[Fe(Mes)_2]_2$, an immediate color change to yellow is observed. The ^1H NMR spectrum of the reaction mixture shows the presence of four broad resonances, presumably due to the formation of monomer **5** (Scheme 3, see also SI, Figure S7). These resonances decrease in intensity upon heating to 85 °C accompanied by the appearance of eight new resonances with increasing intensity over time. Six of those rising resonances are assigned to the doubly yldiide-bridged Fe^{II} dimer **6**, and the residual two resonances correspond to the couple product mesitylene. After 1 h,

DOI: 10.1021/acs.inorgchem.9b01086
Inorg. Chem. 2019, 58, 9358–9367

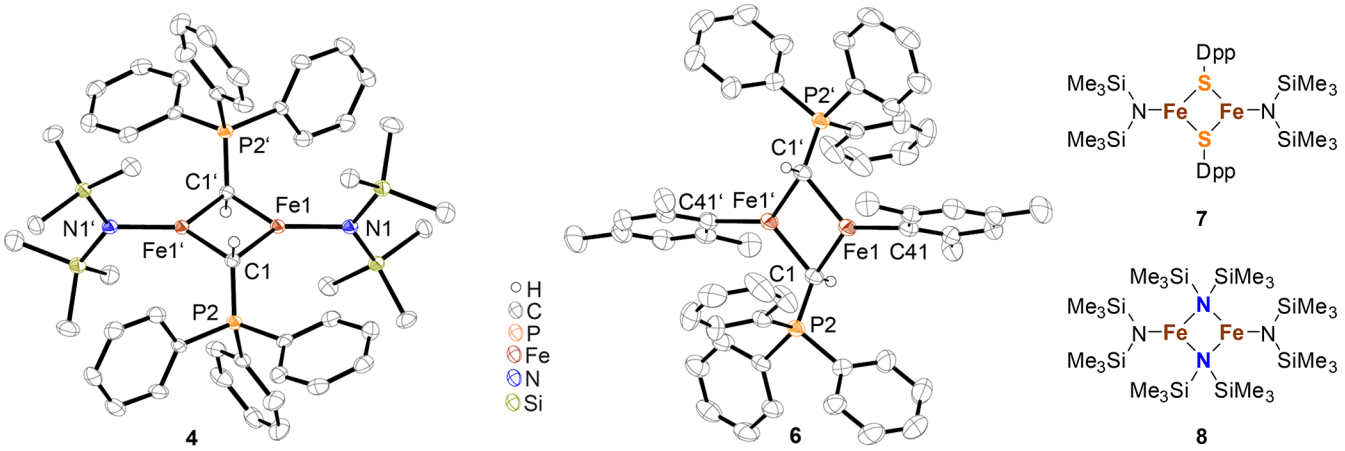

Figure 3. Left: Molecular structures of **4** and **6** (selected hydrogen atoms omitted for clarity, thermal ellipsoids displayed at 50% probability). Right: Related tricoordinated, thiolato- (**7**)[22] and amido-bridged (**8**)[23] Fe^{II} dimers (Dpp: 2,6-di(phenyl)phenyl).

Table 2. Selected Geometrical Parameters for the Crystallographically Characterized Iron Complexes 4 and 6 (Bond Lengths in Å and Angles in Degrees)

	Fe···Fe	Fe–C		Fe–N/C41[a]	C–P	Fe–C–Fe	C1–Fe–C1′	angle sum (Fe)
4	2.5939(12)	2.050(5)	2.046(4)	1.943(4)	1.695(4)	78.58(16)	101.42(16)	360.0(5)
6	2.5826(5)	2.037(2)	2.039(2)	2.037(2)	1.705(2)	78.64(6)	101.36(6)	360.0(1)

[a]C41 atom in complex **6**.

quantitative conversion to **6** is observed, resulting in a deep brown reaction solution from which brown needle-shaped crystals are isolated after layering it with *n*-hexane (yield: 60%). Attempts to isolate analogous Fe_2C_2-dimers from reactions of **1b** and **1c** with with $[Fe(Mes)_2]_2$ were not successful. The molecular structures of **4** and **6** display centrosymmetric Fe dimers, containing a Fe_2C_2-diamond core (Figure 3). A distorted trigonal planar bonding environment is observed for the iron atoms (angle sum around Fe: 360°, see Table 2), whereas the endocyclic C atoms render a distorted tetrahedral geometry. The Fe–C bonds at 2.050(5) Å and 2.046(4) Å in **4** and 2.037(2) Å and 2.039(2) Å in **6** are slightly shorter than those found in the precursors **2a** and **2b**. However, they are significantly longer than those observed in the alkylidene bridged Fe^{II} dimer D reported by Holland et al. (Chart 1, Fe–C 1.973(6) Å, 1.956(6) Å)[14] and are of a comparable length to those observed in the nitrogenase FeMoco (averaged: 2.00 Å).[2a] Remarkable is the very acute Fe–C–Fe angle in **4** (78.58(16)°) and **6** (78.64(6)°). For comparison, the related and literature known thiolato- and amido-bridged Fe^{II} dimers **7** and **8** (Figure 3) render slightly larger Fe–S–Fe (84.34(2)°)[22] and Fe–N–Fe (79.4(1)°)[23] angles, respectively.

The acute Fe–C–Fe angles in **4** and **6** result in an very short Fe···Fe distance of 2.5939(12) Å and 2.5826(5) Å, respectively, being far below the covalent radii of two Fe high spin atoms ($\sum_{covalent\ radii}$: 3.04 Å).[19a] Larger Fe···Fe distances are observed in **7** (3.209(4) Å) and **8** (2.715(1) Å). The ^1H and $^{13}C\{^1H\}$ NMR spectra of **4** and **6** display broad and paramagnetically shifted resonances which are nevertheless unambiguously assignable (see SI).

Noticeably, the resonances of the ylidic C–H protons in **4** and **6** are strongly downfield shifted at δ = 131.58 and 144.31 ppm, respectively. No resonances can be found in the ^{31}P and ^{29}Si NMR (for **4**) spectra due to paramagnetism. The zero field ^{57}Fe Mössbauer spectra of solid **4** and **6** at 80 K show a single quadrupole doublet at δ = 0.35 and 0.24 mm/s with quadrupolar splittings of ΔE_Q = 1.75 and 1.95 mm/s, respectively (Figure 4, top). The solid-state SQUID measurements reveal a temperature dependent effective magnetic moment for **4** and **6** (Figure 4, bottom). Increasing the temperature from 2 to 270 K results in an increase of the μ_{eff} values, indicating very strong antiferromagnetic coupling between the two ferrous ions with S = 2. The coupling constants were determined to be J = −219 cm^{-1} and J = −262 cm^{-1} for **4** and **6**, respectively. To further characterize the

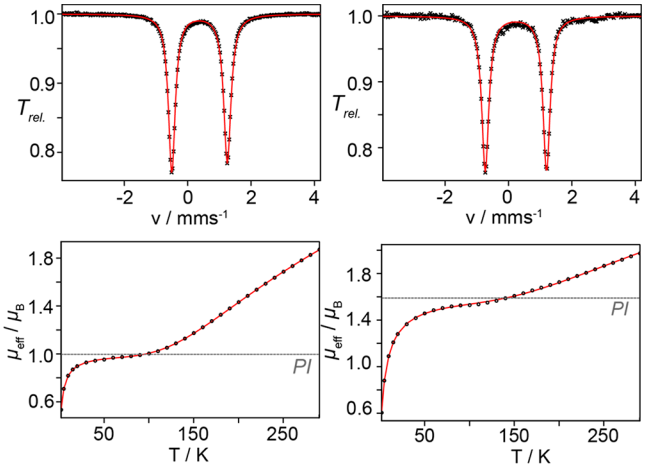

Figure 4. Top: Zero field ^{57}Fe Mössbauer spectra of solid **4** (left) and **6** (right) recorded at 80 K. The solid lines represent fits with δ = 0.35 mm/s and ΔE_Q = 1.75 mm/s for **4** and δ = 0.24 mm/s and ΔE_Q = 1.95 mm/s for **6**. Bottom: Temperature dependent μ_{eff} for **4** (left) and **6** (right) at a field of 1.0 T. The solid lines represent spin-Hamiltonian simulations (fit parameters for **4**: J = −219 cm^{-1}, g1 = g2 = 2.2, PI = paramagnetic impurity = 2.9%, TIP = 1284 × 10^{-6} cm^3 mol^{-1}; fit parameters for **6**: J = −262 cm^{-1}, g1 = g2 = 2.0, PI = 7.5%, TIP = 165 × 10^{-6} cm^3 mol^{-1}).

DOI: 10.1021/acs.inorgchem.9b01086
Inorg. Chem. 2019, 58, 9358–9367

electronic structures of the dimers, **6** was representatively analyzed by Fe K-edge X-ray absorption spectroscopy (XAS).

The normalized XAS spectrum is displayed in Figure 5 and shows a pre-edge feature at 7112.4 eV originating from the

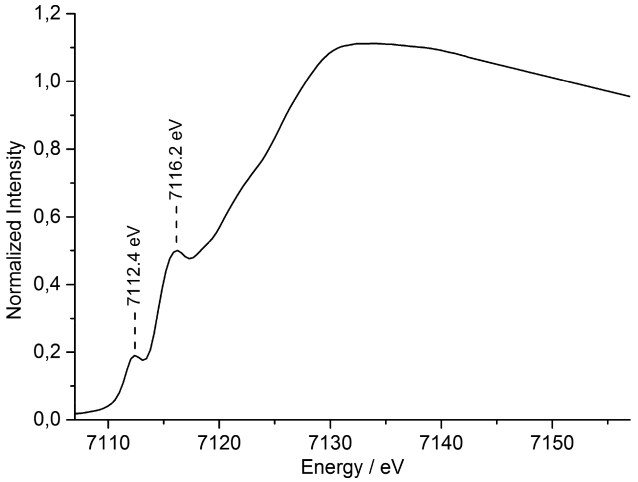

Figure 5. Normalized Fe K-edge XAS spectrum of **6**.

dipole forbidden 1s to 3d transition typically observed for high-spin Fe^{II} centers.[24] The additional intense feature at 7116.2 eV can be assigned to the dipole allowed Fe 1s to $4p_z$ transition, where the ligands around the Fe atoms lie in the *xy* plane. This transition is characteristic for the trigonal planar coordination environment of the Fe atoms.[25] To obtain further insight into the electronic nature of **4** and **6**, broken-symmetry DFT calculations have been performed using the TPSSh functional. The geometry optimized structures of the full models accurately reproduce the molecular structures derived from X-ray crystallography with calculated Fe···Fe distances of 2.568 and 2.557 Å for **4** and **6**, respectively (2.5939(12) Å and 2.5826(5) Å found by X-ray crystallography). Localized magnetic molecular orbitals (LMMO)[26] were chosen to investigate the antiferromagnetic coupling between both iron centers following the analysis concept of Ye et al.[27] The frontier orbitals with significant d character are displayed in Figure 6 for compound **4** (for **6**, see SI, Figure S12). Both iron centers reveal a doubly occupied d_{z^2} orbital, whereas each d_{xz}, d_{yz}, $d_{x^2y^2}$, and d_{xy} orbital is singly occupied, consistent with a high spin Fe^{II} assignment.

The LMMO (Figure 6) for the d_{yz} and d_{xz} pairs shows strong localized iron character (>95%) depending on their spin-state as a result of the antiferromagnetic coupling. In contrast to that, the high-valent $d_{x^2y^2}$ and d_{xy} pairs behave rather covalently with strong interaction between the metals and carbide ligands, respectively. A similar trend of increasing covalency of the high-valent MOs was previously studied by Ye and co-workers for antiferromagnetic coupled mononucleoid transition metal complexes.[27,28] This indicates a mechanism for strong antiferromagnetic coupling in which the Fe···Fe interactions are formed by (a) direct σ-bond interaction of the $d_{x^2y^2}$ pair and (b) the Fe···C interactions provided over the yldiide ligands for both the d_{xy} and the $d_{x^2y^2}$ pair. This magnetic exchange coupling results in a diamagnetic ground state (S_0 = 0), consistent with the SQUID measurements. The Yamaguchi spin-projection formula[29] was used to calculate antiferromagnetic Heisenberg coupling constants of $J = -372$ cm^{-1} and $J = -429$ cm^{-1} for **4** and **6**, respectively, which qualitatively fits

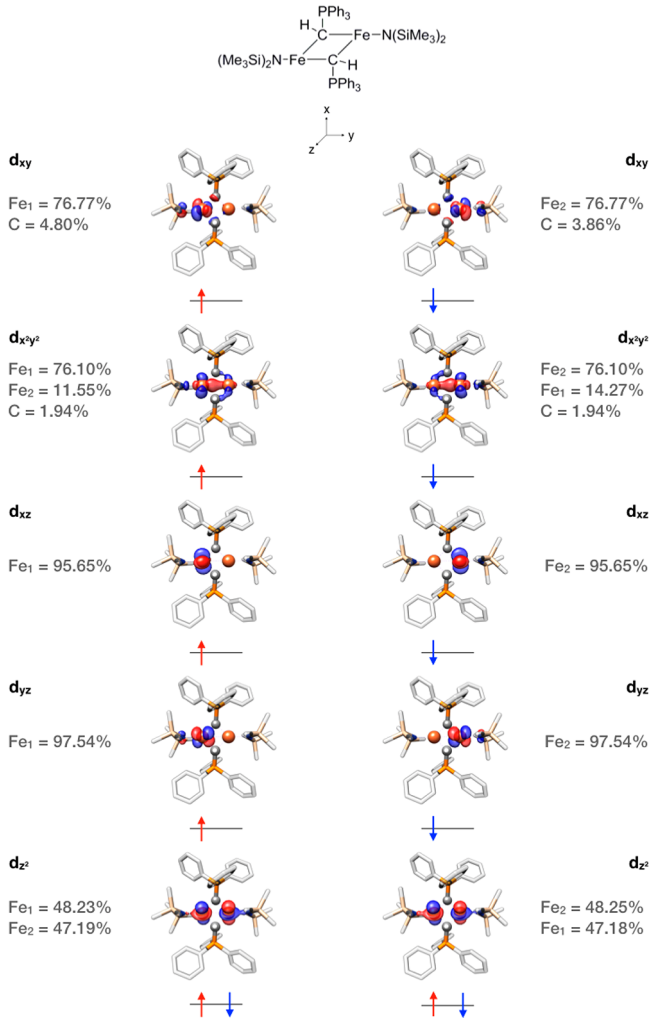

Figure 6. Localized magnetic molecular orbital (LMMO; isosurface-contour value = 0.05) diagram for complex **4**. The spin-density of Fe and the ligand is given for each MO. For the localization, a threshold of 95% was chosen for strongly localized MOs and 80% for bonding MOs, respectively.

with the values observed for the SQUID measurements. We note that a predicted overestimation of the computed *J* values relative to experiment is quite common for single reference DFT methods.[30] The bonding interactions in **4** and **6** were analyzed by Pipek-Mezey localized orbitals displaying a strong Fe−C interaction ($B_{Fe-C} > 0.65$), whereas the Fe−Fe interaction ($B_{Fe-Fe} < 0.18$) is comparatively weak, additionally attested by the Mayer bond-order analysis (see SI, Table S2).[31] The endocyclic Fe−C bonds reveal "pear shaped" localized orbitals that indicate a strong polarization of these bonds where the binding pairs of electrons are mainly localized on the bridging C atoms (Figure 7). This is further reflected by the position of the charge centroid depicted as small red dots centered at the carbon atoms. The depicted localized orbitals are comprised of 19−26% Fe character and 81−74% C character.

CONCLUSION

The synthesis of the doubly yldiide bridged Fe^{II} dimers **4** and **6** is presented facilitated by the self-protolysis reaction of low coordinated ylide-Fe^{II} high-spin complexes **2a**−**2c**. Dimers **4** and **6** represent the first examples of yldiide-supported Fe_2C_2-

DOI: 10.1021/acs.inorgchem.9b01086
Inorg. Chem. 2019, 58, 9358−9367

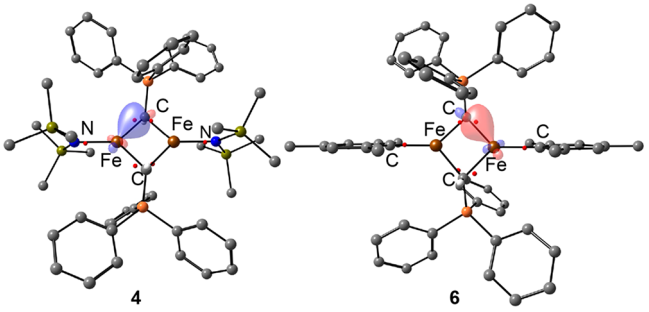

Figure 7. Isosurface plots of Pipek−Mezey localized orbitals for the Fe−C interactions in **4** and **6**. Charge centroids are shown as red dots. Each dot accounts for two electrons.

diamond cores. Very acute Fe−C−Fe angles are observed that result in short Fe···Fe distances. XAS confirms both the high spin Fe^{II} configuration and its trigonal planar bonding environment. The Fe^{II} centers are strongly antiferromagnetically coupled via the yldiide bridges to give a diamagnetic ground state as evidenced by SQUID magnetometry. Highly polarized Fe−C bonds are identified where the bonding pairs of electrons are mostly centered at the μ_2-C ligands. The use of ylides as μ_2-C ligand building blocks formed in a self-protolysis reaction is a very powerful synthetic strategy to access μ-C ligated multinuclear iron complexes. The introduction of additional S-based ligands into yldiide bridged Fe^{II} dimers would yield very promising synthetic model systems for nitrogenase. The synthesis of such sulfur-ligated $[Fe_2C_2]$ clusters is an ongoing research subject in our group.

EXPERIMENTAL SECTION

General Remarks. All manipulations were performed in a Glovebox (MBrown Labmaster pro ECO) under an atmosphere of nitrogen or using Schlenk techniques under an atmosphere of purified argon. Dry, oxygen-free solvents (CH_2Cl_2, CH_3CN, C_6H_5F (distilled from CaH_2); Et_2O, toluene, THF (distilled from potassium/benzophenone); and *n*-hexane and *n*-pentane (distilled from potassium)) were employed. Deuterated benzene (C_6D_6) was purchased from Sigma-Aldrich and distilled from potassium/benzophenone. Benzonitrile (PhCN) and hexamethyldisiloxane $(Me_3Si)_2O$ were degassed and recondensed prior to use. Anhydrous deuterated THF (THF-d_8) and dichloromethane (CD_2Cl_2) were purchased from Sigma-Aldrich. All distilled, recondensed, and deuterated solvents were stored over molecular sieves (4 Å). All glassware was oven-dried at 120 °C prior to use. $[Fe(N(SiMe_3)_2)_2]$,[32] $[Fe(Mes)_2]_2$,[13] Ph_3PCH_2 (**1a**),[33] $Ph_3PCH(SiMe_3)$ (**1b**),[33] and 1,3-*iso*-propyl-2-methylenebenzimidazol ($ImCH_2$, **1c**)[34] were prepared according to a literature procedure. NMR spectra were measured on a Bruker AVANCE III HDX, 500 MHz Ascend (^{1}H (500.05 MHz), ^{13}C (125.75 MHz), ^{31}P (202.42 MHz), ^{19}F (470.52 MHz), ^{29}Si (99.34 MHz)). All ^{13}C NMR spectra were exclusively recorded with composite pulse decoupling. If necessary, reported numbers assigning atoms in the ^{13}C spectra were indirectly deduced from the cross-peaks in 2D correlation experiments (HMBC, HSQC). Chemical shifts (δ) are reported in parts per million. Coupling constants (J) are reported in Hz. Melting points were recorded on an electrothermal melting point apparatus in sealed capillaries under a nitrogen atmosphere and are uncorrected. Infrared (IR) spectra were recorded at ambient temperature using a Thermo Scientific Nicolet iS 5 FT IR spectrometer equipped with a temperature stabilized NIR diode laser. An ATR unit (diamond) was used for recording IR spectra. The intensities are reported relative to the most intense peak and are given in parentheses using the following abbreviations: vw = very weak, w = weak, m = medium, s = strong, vs = very strong. Elemental analyses were performed on a Vario MICRO cube Elemental Analyzer from Elementar Analysatorsysteme GmbH in CHNS modus. UV/vis spectra were recorded with a Cary 8454 UV−vis Diode Array System of Agilent Technologies.

SQUID. Magnetic susceptibility data were measured from powder samples of solid material in the temperature range 2−270 K by using a SQUID magnetometer with a field of 1.0 T (MPMS-7, Quantum Design, calibrated with standard palladium reference sample, error < 2%). Sample holders of quartz with an O-ring sealing were used. The SQUID response curves (raw data) have been corrected for holder and solvent contributions by subtracting the corresponding response curves obtained from separate measurements without sample material. The experimental magnetization data obtained from independent simulation of the corrected SQUID response curves were corrected for underlying diamagnetism by use of tabulated Pascal's constants,[35] as well as for temperature-independent paramagnetism (TIP). Magnetic susceptibility data were analyzed and simulated using the julX software written by E. Bill (Max Planck Institute for Chemical Energy Conversion, Mülheim an der Ruhr).

X-ray Absorption Spectroscopy (XAS). Solid **6** was diluted in boron nitride, sealed in an aluminum spacer (1 mm layer thickness) between Kapton tape windows, stored in liquid nitrogen, and kept at this temperature until the measurement. XAS measurements were performed at the Stanford Synchrotron Radiation Lightsource facility (SSRL, beamline 9−3) operated at 3 GeV, with an electron beam current of ∼500 mA. A double-crystal monochromator (DCM) equipped with a Si(220) crystal pair was used to select the energy of the incoming X-rays with an energy resolution ($\Delta E/E$) of $\sim 10^{-4}$. The monochromator was partially detuned (by ∼30% maximum incident flux) to reduce harmonics. A Rh-coated mirror with a cutoff of 9.5 keV was also used to reject higher harmonics. Samples were measured using a 1 × 4 mm^2 (vertical × horizontal) beam at the sample position. The samples were kept at approximately 15 K using a continuous-flow liquid helium cryostat (Oxford Instruments CF1208). The energy of the incident beam was calibrated by measuring the XAS spectrum of an iron foil and setting the first inflection point to 7111.2 eV. Transmission measurements were performed using an N2-filled ion gas chamber, and reference foil measurements were performed simultaneously. Prior to measurements, each sample was checked for signs of radiation damage by performing subsequent 2.5 min scans over the same sample spot. Background subtraction and normalization were performed using the Athena program of the Demeter package.[36] A second-order polynomial was subtracted from the pre-edge and postedge regions to account for the background.

Mössbauer Spectroscopy. Mössbauer spectra were recorded on a conventional spectrometer with an alternating constant acceleration of the γ-source. The minimum experimental line width was 0.24 mm/s (full width at half-height). The sample temperature was maintained constant in an Oxford Instruments Variox cryostat. The ^{57}Co/Rh source (0.6 GBq) was kept at room temperature. Isomer shifts are quoted relative to iron metal at 300 K. Zero field spectra were measured at 80 K. For solid state measurements, the obtained solid was filled into a Delrin capsule in the glovebox. The capsules were frozen in liquid nitrogen directly after discharging from the glovebox. Handling and mounting of the samples was performed under liquid nitrogen. Data simulation was carried out using the program "mf.SL" written by E. Bill (Max Planck Institute for Chemical Energy Conversion, Mülheim an der Ruhr).

Theoretical Calculations. All DFT calculations were performed using the ORCA Quantum Chemistry Package version 4.1.[37] Single point calculations and full geometry optimizations (based on experimental X-ray structures obtained by X-ray diffraction) for **4** and **6** have been performed by unrestricted density functional theory (DFT). The TPSSh functional[38] in combination with the def2-TZVP basis set[39] and D3 dispersion correction[40] has been used. The RIJCOSX approximation was used to speed up all hybrid DFT calculations.[41] Broken-symmetry solutions (for both single-point calculations and geometry optimizations) were derived by first converging the ferromagnetic solution (M_S = 9), then flipping the spins on one side of the iron atom, and finally reconverging to the

DOI: 10.1021/acs.inorgchem.9b01086
Inorg. Chem. 2019, 58, 9358−9367

antiferromagnetic broken symmetry solution with M_s = 0. The localized orbitals were calculated using the Pipek−Mezey scheme.[42]

X-ray Crystal Structure Determination. Suitable single crystals of **2a**−**2c**, **3**, **4**, and **6** were coated with perfluoropolyether (PFO-XR75), picked up with nylon loops, and immediately mounted in the nitrogen cold stream of the diffractometers at 100 K. A Bruker Nonius KappaCCD diffractometer with a Mo-target rotating-anode X-ray source and Incoatec Helios focusing multilayer optics and a Bruker Kappa Mach3 APEX-II diffractometer with a Bruker IμS and Incoatec Helios mirror was used (Mo Kα radiation; λ = 0.71073 Å). Final cell constants were obtained from least-squares fits of setting angles of several thousand strong reflections. Intensity data were corrected for absorption using intensities of redundant reflections using SADABS.[43] The structures were readily solved by direct and Patterson methods and subsequent difference Fourier techniques. The Bruker ShelXTL2[44] software package was used for solution, refinement, and artwork of the structures. All non-hydrogen atoms were anisotropically refined, and hydrogen atoms were placed at calculated positions and refined as riding atoms with isotropic displacement parameters. Crystal and data collection details are given in Tables S3 and S4 (see SI). The $[((SiMe_3)_2N)_2FeC]$ unit of **2a** was found to be severely disordered. A split atom model with restrained bond distances and displacement parameters using the EADP, SAME, and ISOR instructions of ShelXL was refined to account for the disorder (293 restraints; 0.52/0.48 occupation ratio). A $SiMe_3$ group in the structure of **2c** was also disordered and treated similarly (31 restraints; 0.67/0.33 occupation ratio). Crystals of **6** contained a severely disordered fluorobenzene molecule, which was removed using Platon/SQUEEZE.[45]

Preparation of [(Ph$_3$PCH$_2$)Fe(N(SiMe$_3$)$_2$)$_2$] (2a). A solution of $[Fe(N(SiMe_3)_2)_2]$ (1.51 g, 4.00 mmol) in THF (4 mL) was added to a stirring solution of Ph_3PCH_2 (**1a**, 1.11 g, 4.00 mmol) in THF (5 mL), and the resulting light green reaction mixture was stirred for 1 h at ambient temperature. All volatiles were removed *in vacuo* to afford a pale green solid. *n*-Pentane (5 mL) was added to give a pale green solution followed by the addition of $(Me_3Si)_2O$ (4 mL) resulting in the formation of pale green crystalline material. The volume of the reaction mixture was reduced to 1/2 of its volume, and the supernatant was removed by decantation. The crystalline material was washed with $(Me_3Si)_2O$ (3·0.5 mL) and dried *in vacuo* to give **2a** as highly air sensitive, pale green crystals. **2a** slowly decomposes at ambient temperatures by changing its color to brown and therefore needs to be stored at low temperatures (−35 °C). Yield: 2.23 g (85%). mp: 126 °C. IR (ATR, 298 K, in cm^{-1}): 689 (s), 716 (s), 741 (s), 748 (s), 781 (s), 821 (vs), 876 (m), 966 (s), 1112 (w), 1237 (m), 1437 (w), 1486 (vw), 1968 (vw), 2157 (vw), 2441 (vw), 2890 (vw), 2943 (vw). ^{1}H NMR (C_6D_6, 298 K, in ppm): δ 11.15 (6H, br, *o/m*-CH), 9.09 (6H, br, *m/m*-CH), 6.86 (2H, br, CH_2), 4.19 (3H, br, *p*-CH), −3.04 (36H, br, Me_3Si), resonance for CH_2 is not observed. $^{13}C\{^1H\}$ NMR (C_6D_6, 298 K, in ppm): δ 177.4 (6C, br, *o/m*-C), 148.2 (3C, s, *p*-C), 145.1 (6C, br, *o/m*-C4), resonances for CH_2, *i*-C, and Me_3Si are not observed. $^{31}P\{^1H\}$ and $^{29}Si\{^1H\}$ NMR (C_6D_6, 298 K, in ppm): NMR silent. Magnetic susceptibility (Evan's method in *n*-hexane, CD_2Cl_2, 298 K): 4.9 μ_B. UV/vis (*n*-hexane, λ_{max} in nm, ε_M in M^{-1} cm^{-1}): 354 (1125), 266 (8158), 261 (8050), 273 (7435). Mössbauer (80 K, 0.0 T): 0.54 mms^{-1} (ΔE_Q = 0.92 mms^{-1}). Elemental analysis calculated for $C_{31}H_{53}FeN_2PSi_4$: C, 57.03; H, 8.18; N, 4.29. Found: C, 56.92; H, 7.15; N, 4.17; Deviation of the H value (Δ = 1.03) is explained by rapid decomposition of **1a** during sample preparation and injection.

Preparation of [(Ph$_3$PCH(SiMe$_3$))Fe(N(SiMe$_3$)$_2$)$_2$] (2b). Toluene (2 mL) was added to a mixture of $[Fe(N(SiMe_3)_2)_2]$ (376.3 mg, 1.00 mmol) and $Ph_3PCH(SiMe_3)$ (**1b**, 348.5 mg, 1.00 mmol), and the resulting green-yellow solution was stirred for 1 h at ambient temperature. All volatiles were removed *in vacuo* to afford a pale green solid. *n*-Hexane (2 mL) was added to give a suspension, which was stored for 12 h at −35 °C to give large amounts of crystalline, pale green solid. The supernatant was removed by decantation, the crystalline residue was washed with *n*-pentane (0.5 mL) and dried *in vacuo* to give **2b** as analytically pure, highly air sensitive, pale green crystals. Yield: 590 mg (81%). mp: 120 °C. IR (ATR, 298 K, in cm^{-1}): 690 (s), 710 (s), 727 (m), 747 (s), 782 (m), 829 (vs), 875 (m), 958 (s), 1098 (vw), 1239 (m), 1437 (w), 2893 (vw), 2945 (vw). ^{1}H NMR (C_6D_6, 298 K, in ppm): δ 10.94 (6H, br, *o/m*-CH), 7.69 (6H, br, *o/m*-CH), 5.19 (3H, br, *p*-CH), −0.50 (−10.00) (36H, br, Me_3Si), resonance for CHSi is not observed. $^{13}C\{^1H\}$ NMR (C_6D_6, 298 K, in ppm): δ 162.5 (br, C_{Ph}), 140.0 (br, C_{Ph}), resonances for $CH(SiMe_3)$, *i*-C, and Me_3Si are not observed. $^{31}P\{^1H\}$ and $^{29}Si\{^1H\}$ NMR (C_6D_6, 298 K, in ppm): NMR silent. Magnetic susceptibility (Evan's method in toluene-H^8, toluene-*d*^{8}, 298 K): 5.2 μ_B. UV/vis (*n*-hexane, λ_{max} in nm, ε_M in M^{-1} cm^{-1}): 371 (1546), 300 (4079), 264 (6173). Mössbauer (80 K, 0.0 T): 0.55 mms^{-1} (ΔE_Q = 0.73 mms^{-1}). Elemental analysis calculated for $C_{34}H_{61}FeN_2PSi_5$: C, 56.32; H, 8.48; N, 3.86. Found: C, 56.56; H, 8.88; N, 3.75.

Preparation of [(Im)Fe(N(SiMe$_3$)$_2$)$_2$] (2c). 1,3-*iso*-Propyl-2-methylene-benzimidazole (**1c**, 118.7 mg, 0.55 mmol) was added to a stirring solution of $[Fe(N(SiMe_3)_2)_2]$ (206.0 mg, 0.55 mmol) in toluene (2 mL)/ and the resulting yellow solution was stirred for 10 min at ambient temperature. All volatiles were removed *in vacuo* to afford a colorless solid. *n*-Hexane (2 mL) was added to give an almost clear solution that was filtered. $(Me_3Si)_2O$ (2 mL) was added to the filtrate, and the mixture was stored at −35 °C for 7 days to give large amounts of crystalline material. The supernatant was removed by decantation and the residue was dried *in vacuo* to give **2c** as highly air sensitive colorless needles. **2c** slowly decomposes at ambient temperatures by changing its color to brown and therefore needs to be stored at low temperatures (−35 °C).

Yield: 154 mg (52%), mp: decomp.: > 88 °C. IR (ATR, 298 K, in cm^{-1}): 406 (vw), 414 (vw), 421 (vw), 500 (vs), 554 (m), 625 (w), 638 (m), 658 (w), 705 (vw), 731 (w), 739 (w), 781 (vw), 821 (w), 865 (vw), 892 (vw), 942 (vw), 985 (w), 1094 (vw), 1148 (vs), 1203 (vs), 1231 (s), 1353 (vw), 1375 (vw), 1476 (vw), 1489 (vw), 1502 (vw), 1602 (vw), 1625 (vw), 2894 (vw), 2945 (vw), ^{1}H NMR (C_6D_6, 298 K, in ppm): δ −0.6 (12H, br, *i*Pr-CH_3), −1.88 (36H, br, $-N(Si(CH_3)_2)$), −5.24 (4H, br, CH-aryl), −9.16 (2H, br, *i*Pr-CH), the resonance for CH_2 is not observed. $^{13}C\{^1H\}$ NMR (C_6D_6, 298 K, in ppm): NMR-silent. Magnetic susceptibility (Evan's method in toluene-H^8, toluene-*d*^{8}, 298 K): 5.5 μ_B. Mössbauer (80 K, 0.0 T): 0.51 mms^{-1} (ΔE_Q = 1.14 mms^{-1}). Elemental analysis of sufficient quality could not be obtained due to rapid decomposition of **2c** during sample preparation and injection.

Preparation of [(μ-Ph$_3$PCH)Fe(N(SiMe$_3$)$_2$)]$_2$ (4). Method A: Solid **2a** (210 mg, 0.32 mmol) was heated to 135 °C for 12 h. The resulting brown melt containing crystalline material was stored for 24 h at −35 °C. The residual orange-brown crystalline material was washed with CH_2Cl_2 (1 mL) and dried *in vacuo* (yield: 29 mg, 18%). Method B: A solution of Ph_3PCH_2 (**1a**, 110.6 mg, 0.40 mmol) in THF (1 mL) was added to a stirring solution of $[Fe(N(SiMe_3)_2)_2]$ (74.0 mg, 0.2 mmol) in THF (1 mL). The reaction mixture was stirred for 10 min followed by removal of all volatiles *in vacuo*. The yellow, sticky residue was heated to 135 °C for 24 h to give a brown residue. CH_2Cl_2 (1 mL) was added, and the resulting suspension was stored for 1 week at −35 °C. The brown suspension was filtered, and the residue was washed with CH_2Cl_2 (4 × 0.2 mL) and dried *in vacuo* to give an air sensitive, orange-red powder (yield: 27 mg, 28%). mp: decomp. > 285 °C. IR (ATR, 298 K, in cm^{-1}): 403 (vw), 411 (vw), 439 (w), 446 (w), 468 (w), 513 (vs), 536 (s), 579 (vs), 610 (w), 625 (w), 661 (m), 690 (vs), 709 (vs), 743 (s), 788 (m), 817 (vs), 841 (s), 867 (vs), 885 (s), 918 (vw), 929 (vw), 980 (vs), 1003 (w), 1029 (vw), 1100 (m), 1111 (w), 1183 (vw), 1236 (m), 1251 (w), 1435 (m), 1482 (vw), 1981 (vw), 2891 (vw), 2948 (w), 3052 (vw). ^{1}H NMR (C_6D_6, 298 K, in ppm): δ 131.58 (2H, s, CH-PPh_3), 6.66 (12H, br, *o/m*-CH), 6.13 (6H, br, *p*-CH), 4.84 (12H, br, *o/m*-CH), −0.25 (36H, br, $SiMe_3$). $^{13}C\{^1H\}$ NMR (C_6D_6, 298 K, in ppm): δ 133.0 (12C, br, *o/m*-C), 132.9 (6C, br, *p*-C), 130.2 (12C, br, *o/m*-C). $^{31}P\{^1H\}-^{29}Si\{^1H\}$ NMR (C_6D_6, 298 K, in ppm): NMR silent. Mössbauer (80 K, 0.0 T): 0.35 mms^{-1} (ΔE_Q = 1.75 mms^{-1}). Elemental analysis calculated for $C_{50}H_{68}Fe_2N_2P_2Si_4$: C, 61.09; H, 6.97; N, 2.85. Found: C, 60.95; H, 6.84; N, 2.90.

DOI: 10.1021/acs.inorgchem.9b01086
Inorg. Chem. 2019, 58, 9358−9367

Preparation of $[(\mu\text{-}Ph_3PCH)Fe(N(SiMe_3)_2)]_2$ (6). A solution of Ph_3PCH_2 (**1a**, 111 mg, 0.40 mmol) in C_6H_5F (1.5 mL) was added to a stirring solution of $[Fe(Mes)_2]_2$ (118 mg, 0.20 mmol) in C_6H_5F (1.5 mL) to give a yellow solution which was subsequently heated to 85 °C for 4 h. The resulting brown reaction mixture was cooled to ambient temperature and filtered to give a brown solution. Slow vapor diffusion of *n*-hexane into the brown solution yielded deep brown crystals. Yield: 109 mg (60%). mp: decomp. > 320 °C. IR (ATR, 298 K, in cm^{-1}): 738 (m), 748 (s), 837 (m), 882 (vs), 918 (w), 978 (vs), 1026 (w), 1098 (vs), 1161 (w), 1186 (w), 1304 (w), 1363 (w), 1435 (s), 1481 (w), 1588 (w), 1967 (w), 2167 (w), 2898 (w), 3051 (w). ^1H NMR (C_6D_6, 298 K, in ppm): δ 144.32 (2H, br, CH-PPh_3), 13.60 (4H, br, *m*-CH(mesityl)), 11.09 (6H, br, *p*-CH_3(mesityl)), 6.32 (12H, br, *m*/*o*-CH(PPh_3)), 6.06 (12H, br, *m*/*o*-CH(PPh_3)), 5.98 (6H, t, J_{HH} = 7.0 Hz, *p*-CH(PPh_3)), −0.58 (12H, br, *o*-CH_3(mesityl)). $^{13}C\{^1H\}$ NMR (C_6D_6, 298 K, in ppm): δ 277.4 (4C, br, *o*-C(mesityl)), 207.1 (6C, br, *i*-C(PPh_3)), 180.4 (2C, br, *p*-C(mesityl)), 139.3 (12C, br, *o*-/m-CH(PPh_3)), 132.6 (6C, br, *p*-CH(PPh_3)), 130.0 (12C, br, *o*-/*p*-CH(PPh_3)), 94.8 (4C, br, *m*-CH(mesityl)), 38.5 (4C, br, *o*-CH_3(mesityl)), 9.0 (2C, br, *p*-CH_3(mesityl)). $^{31}P\{^1H\}$ NMR (C_6D_6, 298 K, in ppm): NMR silent. UV/vis (THF, λ_{max} in nm, ε_M in M^{-1} cm^{-1}): 470 (3513, sh), 413 (7790), 344 (9021), 296 (23150). Mössbauer (80 K, 0.0 T): 0.24 mms^{-1} (ΔE_Q = 1.95 mms^{-1}). Elemental analysis calculated for $C_{56}H_{54}Fe_2P_2$: C, 74.68; H, 6.04. Found: C, 74.29; H, 6.49.

■ ASSOCIATED CONTENT

Supporting Information

The Supporting Information is available free of charge on the ACS Publications website at DOI: 10.1021/acs.inorgchem.9b01086.

NMR spectra of **2a**−**2c**, **4**, and **6**; time- and temperature dependent reaction of **1a** with $[Fe(Mes)_2]_2$ monitored by ^1H NMR spectroscopy; reaction of **2a** with benzonitrile; Mössbauer spectra of **2a**−**2c**; molecular orbital diagram for **6**; Mayer bond-order analysis (MBOA) of complexes **4** and **6**; Orca DFT input file for full geometry optimization for **4** and **6** (broken symmetry); Orca DFT input file for localized orbital analysis for **4** and **6**; Cartesian coordinates of the fully geometry optimized structure of **4** (broken symmetry); Cartesian coordinates of the fully geometry optimized structure of **6** (broken symmetry); X-ray crystallographic data collection and refinement of the structures (PDF)

Accession Codes

CCDC 1901687−1901692 contain the supplementary crystallographic data for this paper. These data can be obtained free of charge via www.ccdc.cam.ac.uk/data_request/cif, or by emailing data_request@ccdc.cam.ac.uk, or by contacting The Cambridge Crystallographic Data Centre, 12 Union Road, Cambridge CB2 1EZ, UK; fax: + 44 1223 336033.

■ AUTHOR INFORMATION

Corresponding Authors

*E-mail: Sivathmeehan.Yogendra@cec.mpg.de.
*E-mail: Serena.DeBeer@cec.mpg.de.

ORCID

Thomas Weyhermüller: 0000-0002-0399-7999
Serena DeBeer: 0000-0002-5196-3400

Notes

The authors declare no competing financial interest.

■ ACKNOWLEDGMENTS

The Max Planck Society is acknowledged for funding. J.J. Weigand (TU Dresden) is thanked for elemental analysis. Casey van Stappen, Natalia Levin Rojas, and Patricia Rodriguez are thanked for XAS data collection. Portions of this research were carried out at the Stanford Synchrotron Radiation Lightsource (SSRL), a national user facility operated by Stanford University on behalf of the U.S. Department of Energy, Office of Basic Energy Sciences. The SSRL Structural Molecular Biology Program is supported by DOE, Biological and Environmental Research, and NIH, National Center for Research Resources, Biomedical Technology Program.

■ REFERENCES

(1) (a) Hoffman, B. M.; Lukoyanov, D.; Yang, Z.-Y.; Dean, D. R.; Seefeldt, L. C. Mechanism of Nitrogen Fixation by Nitrogenase: The Next Stage. *Chem. Rev.* **2014**, *114* (8), 4041−4062. (b) Burgess, B. K.; Lowe, D. J. Mechanism of Molybdenum Nitrogenase. *Chem. Rev.* **1996**, *96* (7), 2983−3012.

(2) (a) Einsle, O.; Tezcan, F. A.; Andrade, S. L. A.; Schmid, B.; Yoshida, M.; Howard, J. B.; Rees, D. C. Nitrogenase MoFe-Protein at 1.16 Å Resolution: A Central Ligand in the FeMo-Cofactor. *Science* **2002**, *297* (5587), 1696−1700. (b) Lancaster, K. M.; Roemelt, M.; Ettenhuber, P.; Hu, Y.; Ribbe, M. W.; Neese, F.; Bergmann, U.; DeBeer, S. X-ray Emission Spectroscopy Evidences a Central Carbon in the Nitrogenase Iron-Molybdenum Cofactor. *Science* **2011**, *334* (6058), 974. (c) Spatzal, T.; Aksoyoglu, M.; Zhang, L.; Andrade, S. L. A.; Schleicher, E.; Weber, S.; Rees, D. C.; Einsle, O. Evidence for Interstitial Carbon in Nitrogenase FeMo Cofactor. *Science* **2011**, *334* (6058), 940−940.

(3) (a) Wiig, J. A.; Hu, Y.; Lee, C. C.; Ribbe, M. W. Radical SAM-Dependent Carbon Insertion into the Nitrogenase M-Cluster. *Science* **2012**, *337* (6102), 1672−1675. (b) Wiig, J. A.; Hu, Y.; Ribbe, M. W. Refining the pathway of carbide insertion into the nitrogenase M-cluster. *Nat. Commun.* **2015**, *6*, 8034. (c) Lancaster, K. M.; Hu, Y.; Bergmann, U.; Ribbe, M. W.; DeBeer, S. X-ray Spectroscopic Observation of an Interstitial Carbide in NifEN-Bound FeMoco Precursor. *J. Am. Chem. Soc.* **2013**, *135* (2), 610−612.

(4) (a) Wiig, J. A.; Lee, C. C.; Hu, Y.; Ribbe, M. W. Tracing the Interstitial Carbide of the Nitrogenase Cofactor during Substrate Turnover. *J. Am. Chem. Soc.* **2013**, *135* (13), 4982−4983. (b) Rees, J. A.; Bjornsson, R.; Kowalska, J. K.; Lima, F. A.; Schlesier, J.; Sippel, D.; Weyhermuller, T.; Einsle, O.; Kovacs, J. A.; DeBeer, S. Comparative electronic structures of nitrogenase FeMoco and FeVco. *Dalton Trans.* **2017**, *46* (8), 2445−2455.

(5) (a) Dance, I. The Mechanistically Significant Coordination Chemistry of Dinitrogen at FeMo-co, the Catalytic Site of Nitrogenase. *J. Am. Chem. Soc.* **2007**, *129* (5), 1076−1088. (b) Rittle, J.; Peters, J. C. Fe−N2/CO complexes that model a possible role for the interstitial C atom of FeMo-cofactor (FeMoco). *Proc. Natl. Acad. Sci. U. S. A.* **2013**, *110* (40), 15898−15903. (c) Creutz, S. E.; Peters, J. C. Catalytic Reduction of N2 to NH3 by an Fe−N2 Complex Featuring a C-Atom Anchor. *J. Am. Chem. Soc.* **2014**, *136* (3), 1105−1115.

(6) Siegbahn, P. E. M. Model Calculations Suggest that the Central Carbon in the FeMo-Cofactor of Nitrogenase Becomes Protonated in the Process of Nitrogen Fixation. *J. Am. Chem. Soc.* **2016**, *138* (33), 10485−10495.

(7) Čorić, I.; Holland, P. L. Insight into the Iron−Molybdenum Cofactor of Nitrogenase from Synthetic Iron Complexes with Sulfur, Carbon, and Hydride Ligands. *J. Am. Chem. Soc.* **2016**, *138* (23), 7200−7211.

(8) (a) Kuppuswamy, S.; Wofford, J. D.; Joseph, C.; Xie, Z.-L.; Ali, A. K.; Lynch, V. M.; Lindahl, P. A.; Rose, M. J. Structures, Interconversions, and Spectroscopy of Iron Carbonyl Clusters with an Interstitial Carbide: Localized Metal Center Reduction by Overall Cluster Oxidation. *Inorg. Chem.* **2017**, *56* (10), 5998−6012.

DOI: 10.1021/acs.inorgchem.9b01086
Inorg. Chem. 2019, 58, 9358−9367

(b) Muetterties, E. L. Molecular Metal Clusters as Catalysts. *Catal. Rev.: Sci. Eng.* **1981**, *23* (1−2), 69−87. (c) Holt, E. M.; Whitmire, K. H.; Shriver, D. F. The role of metal cluster interactions in the proton-induced reduction of CO. the crystal structures of [PPN]{HFe4-(CO)12} and HFe4(CO)12(η-COCH3). *J. Organomet. Chem.* **1981**, *213* (1), 125−137. (d) Boehme, R. F.; Coppens, P. The structure of a tetranuclear metal cluster with a four-coordinate carbide carbon atom: bis(benzyltrimethylammonium) [mu]-carbido-dodeca-carbonyl-tetra-hedro-tetraferrate. *Acta Crystallogr., Sect. B: Struct. Crystallogr. Cryst. Chem.* **1981**, *37* (10), 1914−1916. (e) Reinholdt, A.; Majer, S. H.; Gelardi, R. M.; MacMillan, S. N.; Hill, A. F.; Wendt, O. F.; Lancaster, K. M.; Bendix, J. An Approach to Carbide-Centered Cluster Complexes. *Inorg. Chem.* **2019**, *58*, 4812.

(9) (a) Knauer, W.; Beck, W. Carbid-verbrückte Komplexe [HB(pz)3(OC)2Mo≡C-Pt(PPh3)2Br], [(TPP)Fe≡C-M(CO)4-M-(CO)5] (M = Mn, Re), [(TPP)Fe═C═Cr(CO)5] und (TPP)Fe═C═Fe(CO)4] (pz = 3,5-dimethylpyrazol-1-yl; TPP = Tetra-phenyl-porphyrinat) aus Halogeno-Carbin und -Carben-Komplexen. *Z. Anorg. Allg. Chem.* **2008**, *634* (12−13), 2241−2245. (b) Galich, L.; Kienast, A.; Hückstädt, H.; Homborg, H. Synthesen, spektroskopische Eigenschaften und Kristallstrukturen zweikerniger homo- und heteroleptischer μ-Carbido-Komplexe von Eisen(IV) mit Phthalocya-ninat- und Tetraphenylporphyrinat-Liganden. *Z. Anorg. Allg. Chem.* **1998**, *624* (7), 1235−1242. (c) Kienast, A.; Bruhn, C.; Homborg, H. Darstellung, Eigenschaften und Kristallstruktur von μ-Carbidodi-(pyridinphthalocyaninato(2−)eisen(IV)) und -ruthenium(IV). *Z. Anorg. Allg. Chem.* **1997**, *623* (1−6), 967−972. (d) Rossi, G.; Goedken, V. L.; Ercolani, C. [small micro]-Carbido-bridged iron phthalocyanine dimers: synthesis and characterization. *J. Chem. Soc., Chem. Commun.* **1988**, No. 1, 46−47. (e) Mansuy, D.; Lecomte, J. P.; Chottard, J. C.; Bartoli, J. F. Formation of a complex with a carbide bridge between two iron atoms from the reaction of (tetraphenylporphyrin)iron(II) with carbon tetraiodide. *Inorg. Chem.* **1981**, *20* (9), 3119−3121. (f) English, D. R.; Hendrickson, D. N.; Suslick, K. S. Moessbauer spectra of oxidized iron porphyrins. *Inorg. Chem.* **1983**, *22* (2), 367−368.

(10) Vollmer, G. Y.; Wallasch, M. W.; Saurenz, D.; Eger, T. R.; Bauer, H.; Wolmershäuser, G.; Prosenc, M. H.; Sitzmann, H. Benzylidyne Bridges from Diphenylacetylene and a Methylidyne Bridge from Methylmagnesium Chloride. *Organometallics* **2015**, *34* (3), 644−652.

(11) (a) Ni, C.; Power, P. P. Methyl-Bridged Transition Metal Complexes (M = Cr−Fe) Supported by Bulky Terphenyl Ligands. *Organometallics* **2009**, *28* (22), 6541−6545. (b) Müller, H.; Seidel, W.; Görls, H. Zur Chemie des Dimesityleisens: VI. Die struktur von tetramesityldieisen. *J. Organomet. Chem.* **1993**, *445* (1), 133−136.

(12) Sun, C. L.; Krause, H.; Fürstner, A. A Practical Procedure for Iron-Catalyzed Cross-Coupling Reactions of Sterically Hindered Aryl-Grignard Reagents with Primary Alkyl Halides. *Adv. Synth. Catal.* **2014**, *356*, 1281−1291.

(13) Klose, A.; Solari, E.; Floriani, C.; Chiesi-Villa, A.; Rizzoli, C.; Re, N. Magnetic Properties Diagnostic for the Existence of Iron(II)-Iron(II) Bonds in Dinuclear Complexes Which Derive from Stepwise Insertion Reactions on Unsupported Iron-Aryl Bonds. *J. Am. Chem. Soc.* **1994**, *116* (20), 9123−9135.

(14) Reesbeck, M. E.; Grubel, K.; Kim, D.; Brennessel, W. W.; Mercado, B. Q.; Holland, P. L. Diazoalkanes in Low-Coordinate Iron Chemistry: Bimetallic Diazoalkyl and Alkylidene Complexes of Iron(II). *Inorg. Chem.* **2017**, *56* (3), 1019−1022.

(15) (a) Byrne, P. A.; Gilheany, D. G. The modern interpretation of the Wittig reaction mechanism. *Chem. Soc. Rev.* **2013**, *42* (16), 6670−6696. (b) Gessner, V. H. Reactivity and Applications of α-Metalated Ylides. In *Modern Ylide Chemistry: Applications in Ligand Design, Organic and Catalytic Transformations*; Gessner, V. H., Ed.; Springer International Publishing: Cham, 2018; pp 117−155. (c) Roy, M. M. D.; Rivard, E. Pushing Chemical Boundaries with N-Heterocyclic Olefins (NHOs): From Catalysis to Main Group Element Chemistry. *Acc. Chem. Res.* **2017**, *50* (8), 2017−2025.

(16) Clavier, H.; Nolan, S. P. Percent buried volume for phosphine and N-heterocyclic carbene ligands: steric properties in organo-metallic chemistry. *Chem. Commun.* **2010**, *46* (6), 841−861.

(17) (a) Sciarone, T. J. J.; Meetsma, A.; Hesssen, B.; Teuben, J. H. Benzyl anion abstraction from a ([small beta]-diiminato)Fe(ii) benzyl complex. *Chem. Commun.* **2002**, No. 15, 1580−1581. (b) Smith, J. M.; Lachicotte, R. J.; Holland, P. L. Three-Coordinate, 12-Electron Organometallic Complexes of Iron(II) Supported by a Bulky β-Diketiminate Ligand: Synthesis and Insertion of CO To Give Square-Pyramidal Complexes. *Organometallics* **2002**, *21* (22), 4808−4814. (c) Andres, H.; Bominaar, E. L.; Smith, J. M.; Eckert, N. A.; Holland, P. L.; Münck, E. Planar Three-Coordinate High-Spin FeII Complexes with Large Orbital Angular Momentum: Mössbauer, Electron Paramagnetic Resonance, and Electronic Structure Studies. *J. Am. Chem. Soc.* **2002**, *124* (12), 3012−3025.

(18) Maddock, L. C. H.; Cadenbach, T.; Kennedy, A. R.; Borilovic, I.; Aromí, G.; Hevia, E. Accessing Sodium Ferrate Complexes Containing Neutral and Anionic N-Heterocyclic Carbene Ligands: Structural, Synthetic, and Magnetic Insights. *Inorg. Chem.* **2015**, *54* (18), 9201−9210.

(19) (a) Cordero, B.; Gomez, V.; Platero-Prats, A. E.; Reves, M.; Echeverria, J.; Cremades, E.; Barragan, F.; Alvarez, S. Covalent radii revisited. *Dalton Trans.* **2008**, No. 21, 2832−2838. (b) Yogendra, S.; Hennersdorf, F.; Bauzá, A.; Frontera, A.; Fischer, R.; Weigand, J. J. Donor−acceptor interactions in tri(phosphonio)methanide dications [(Ph3P)2CP(X)Ph2]2+ (X = H, Me, CN, NCS, OH, Cl, OTf, F). *Dalton Trans.* **2017**, *46* (44), 15503−15511.

(20) Streitwieser, A..; Kosower, E. M.; Heathcock, C. H. *Introduction to Organic Chemistry*, 4th ed.; Prentice Hall, 1992; p 574.

(21) Evans, D. F. 400. The determination of the paramagnetic susceptibility of substances in solution by nuclear magnetic resonance. *J. Chem. Soc.* **1959**, No. 0, 2003−2005.

(22) Ohta, S.; Ohki, Y.; Ikagawa, Y.; Suizu, R.; Tatsumi, K. Synthesis and characterization of heteroleptic iron(II) thiolate complexes with weak iron−arene interactions. *J. Organomet. Chem.* **2007**, *692* (21), 4792−4799.

(23) Olmstead, M. M.; Power, P. P.; Shoner, S. C. Three-coordinate iron complexes: x-ray structural characterization of the iron amide-bridged dimers [Fe(NR2)2]2 (R = SiMe3, C6H5) and the adduct Fe[N(SiMe3)2]2(THF) and determination of the association energy of the monomer Fe{N(SiMe3)2}2 in solution. *Inorg. Chem.* **1991**, *30* (11), 2547−2551.

(24) (a) Kowalska, J. K.; Hahn, A. W.; Albers, A.; Schiewer, C. E.; Bjornsson, R.; Lima, F. A.; Meyer, F.; DeBeer, S. X-ray Absorption and Emission Spectroscopic Studies of [L2Fe2S2]n Model Complexes: Implications for the Experimental Evaluation of Redox States in Iron−Sulfur Clusters. *Inorg. Chem.* **2016**, *55* (9), 4485−4497. (b) Westre, T. E.; Kennepohl, P.; DeWitt, J. G.; Hedman, B.; Hodgson, K. O.; Solomon, E. I. A Multiplet Analysis of Fe K-Edge 1s → 3d Pre-Edge Features of Iron Complexes. *J. Am. Chem. Soc.* **1997**, *119* (27), 6297−6314.

(25) Chandrasekaran, P.; Chiang, K. P.; Nordlund, D.; Bergmann, U.; Holland, P. L.; DeBeer, S. Sensitivity of X-ray Core Spectroscopy to Changes in Metal Ligation: A Systematic Study of Low-Coordinate, High-Spin Ferrous Complexes. *Inorg. Chem.* **2013**, *52* (11), 6286−6298.

(26) (a) Neese, F. Importance of Direct Spin−Spin Coupling and Spin-Flip Excitations for the Zero-Field Splittings of Transition Metal Complexes: A Case Study. *J. Am. Chem. Soc.* **2006**, *128* (31), 10213−10222. (b) Knizia, G. Intrinsic Atomic Orbitals: An Unbiased Bridge between Quantum Theory and Chemical Concepts. *J. Chem. Theory Comput.* **2013**, *9* (11), 4834−4843.

(27) Mondal, B.; Neese, F.; Bill, E.; Ye, S. F. Electronic Structure Contributions of Non-Herne Oxo-Iron(V) Complexes to the Reactivity. *J. Am. Chem. Soc.* **2018**, *140* (30), 9531−9544.

(28) Wang, D.; Leng, X.; Ye, S.; Deng, L. Substrate Redox Non-innocence Inducing Stepwise Oxidative Addition Reaction: Nitro-soarene C-N Bond Cleavage on Low-Coordinate Cobalt(0) Species. *J. Am. Chem. Soc.* **2019**, *141* (19), 7731−7735.

DOI: 10.1021/acs.inorgchem.9b01086
Inorg. Chem. 2019, 58, 9358−9367

(29) Yamanaka, S.; Kawakami, T.; Nagao, H.; Yamaguchi, K. Effective exchange integrals for open-shell species by density functional methods. *Chem. Phys. Lett.* **1994**, *231* (1), 25−33.
(30) (a) David, G.; Wennmohs, F.; Neese, F.; Ferré, N. Chemical Tuning of Magnetic Exchange Couplings Using Broken-Symmetry Density Functional Theory. *Inorg. Chem.* **2018**, *57* (20), 12769−12776. (b) Neese, F. Prediction of molecular properties and molecular spectroscopy with density functional theory: From fundamental theory to exchange-coupling. *Coord. Chem. Rev.* **2009**, *253* (5), 526−563. (c) Neese, F.; Petrenko, T.; Ganyushin, D.; Olbrich, G. Advanced aspects of ab initio theoretical optical spectroscopy of transition metal complexes: Multiplets, spin-orbit coupling and resonance Raman intensities. *Coord. Chem. Rev.* **2007**, *251* (3), 288−327.
(31) Bridgeman, A. J.; Cavigliasso, G.; Ireland, L. R.; Rothery, J. The Mayer bond order as a tool in inorganic chemistry. *J. Chem. Soc. Dalton* **2001**, No. 14, 2095−2108.
(32) Andersen, R. A.; Faegri, K.; Green, J. C.; Haaland, A.; Lappert, M. F.; Leung, W. P.; Rypdal, K. Synthesis of bis[bis(trimethylsilyl)-amido]iron(II). Structure and bonding in M[N(SiMe3)2]2 (M = manganese, iron, cobalt): two-coordinate transition-metal amides. *Inorg. Chem.* **1988**, *27* (10), 1782−1786.
(33) Bestmann, H. J.; Bomhard, A.; Dostalek, R.; Pichl, R.; Riemer, R.; Zimmermann, R. Phosphinalkylene, 51; Synthese und Reaktionen von [1-(Trialkylsilyl)alkyliden]triphenylphosphoranen. *Synthesis* **1992**, *1992* (08), 787−792.
(34) Chen, W. C.; Shen, J. S.; Jurca, T.; Peng, C. J.; Lin, Y. H.; Wang, Y. P.; Shih, W. C.; Yap, G. P. A.; Ong, T. G. Expanding the Ligand Framework Diversity of Carbodicarbenes and Direct Detection of Boron Activation in the Methylation of Amines with CO2. *Angew. Chem., Int. Ed.* **2015**, *54* (50), 15207−15212.
(35) Bain, G. A.; Berry, J. F. Diamagnetic Corrections and Pascal's Constants. *J. Chem. Educ.* **2008**, *85* (4), 532.
(36) Ravel, B.; Newville, M. ATHENA, ARTEMIS, HEPHAESTUS: data analysis for X-ray absorption spectroscopy using IFEFFIT. *J. Synchrotron Radiat.* **2005**, *12* (4), 537−541.
(37) (a) Neese, F. The ORCA program system. *WIREs Comput. Mol. Sci.* **2012**, *2* (1), 73−78. (b) Neese, F. Software update: the ORCA program system, version 4.0. *WIREs Comput. Mol. Sci.* **2018**, *8* (1), e1327.
(38) (a) Tao, J.; Perdew, J. P.; Staroverov, V. N.; Scuseria, G. E. Climbing the Density Functional Ladder: Nonempirical Meta–Generalized Gradient Approximation Designed for Molecules and Solids. *Phys. Rev. Lett.* **2003**, *91* (14), 146401. (b) Staroverov, V. N.; Scuseria, G. E.; Tao, J.; Perdew, J. P. Comparative assessment of a new nonempirical density functional: Molecules and hydrogen-bonded complexes. *J. Chem. Phys.* **2003**, *119* (23), 12129−12137.
(39) (a) Weigend, F.; Ahlrichs, R. Balanced basis sets of split valence, triple zeta valence and quadruple zeta valence quality for H to Rn: Design and assessment of accuracy. *Phys. Chem. Chem. Phys.* **2005**, *7* (18), 3297−3305. (b) Pantazis, D. A.; Chen, X.-Y.; Landis, C. R.; Neese, F. All-Electron Scalar Relativistic Basis Sets for Third-Row Transition Metal Atoms. *J. Chem. Theory Comput.* **2008**, *4* (6), 908−919.
(40) (a) Grimme, S.; Antony, J.; Ehrlich, S.; Krieg, H. A consistent and accurate ab initio parametrization of density functional dispersion correction (DFT-D) for the 94 elements H-Pu. *J. Chem. Phys.* **2010**, *132* (15), 154104. (b) Grimme, S.; Ehrlich, S.; Goerigk, L. Effect of the damping function in dispersion corrected density functional theory. *J. Comput. Chem.* **2011**, *32* (7), 1456−1465.
(41) (a) Izsák, R.; Neese, F. An overlap fitted chain of spheres exchange method. *J. Chem. Phys.* **2011**, *135* (14), 144105. (b) Neese, F.; Wennmohs, F.; Hansen, A.; Becker, U. Efficient, approximate and parallel Hartree−Fock and hybrid DFT calculations. A 'chain-of-spheres' algorithm for the Hartree−Fock exchange. *Chem. Phys.* **2009**, *356* (1), 98−109.
(42) Pipek, J.; Mezey, P. G. A fast intrinsic localization procedure applicable for ab initio and semiempirical linear combination of atomic orbital wave functions. *J. Chem. Phys.* **1989**, *90* (9), 4916−4926.
(43) Sheldrick, G. M. *SADABS, Bruker−Siemens Area Detector Absorption and Other Correction*, version 2012/1; University of Göttingen: Germany, 2012.
(44) *ShelXTL MP*, Vers. 2013-2; Bruker AXS Inc., 1993−2013.
(45) Platon/Squeeze: Spek, A. L. *Acta Crystallogr., Sect. D: Biol. Crystallogr.* **2009**, *D65*, 148−155. Spek, A. L. *Platon − A Multipurpose Crystallographic Tool*; Utrecht University: Utrecht, The Netherlands, 2011.

DOI: 10.1021/acs.inorgchem.9b01086
Inorg. Chem. 2019, 58, 9358−9367